

Original Research

Investigation of the Effect of Urban Parks on the Urban Heat Island with Remote Sensing and GIS

Mert Akoğlu^{1*}, Şeyma Berk Acet²

¹Department of Landscape Architecture, Faculty of Architecture, Süleyman Demirel University, Isparta, Turkey

²Department of Remote Sensing and Geographic Information Systems, Institute of Graduate Programs, Eskişehir Technical University, Eskişehir, Turkey

Received: 25 May 2022

Accepted: 14 March 2023

Abstract

The rapid urbanization of cities has led to a radical change in the use of land in cities with the accompanying climate change. It has formed urban heat islands, which have begun to be characterized by climatic conditions such as temperature, precipitation, humidity and wind that differ from the surroundings of cities. It is observed that the heat island effect is felt more intensively day by day, especially in large cities such as Ankara, where urbanization is increasing. It is possible to determine and analyze the urban heat island effect using satellite technologies. Google Earth Engine (GEE) is an online platform that enables remote sensing users to efficiently perform big data analysis without increasing the demand for local computing resources. In this study, NDVI (Normalized Difference Vegetation Index) and LST (Land Surface Temperature) spectral indices were analyzed using Google Earth Engine, remote sensing and GIS techniques in four important parks with different sizes and plant diversity located in the urban area of Ankara. The NDVI and LST results were then analyzed with zonal statistics. Although studies have shown that urban parks create a temperature change effect of about 1°C, it has been observed that the temperature difference is about 3 °C in this study. These results show that the urban heat island effect is increasing in Ankara province, where the effects of climate change are seen rapidly.

Keywords: urban heat island, Ankara, urban park, remote sensing, GIS

Introduction

Urban areas are becoming more and more important as 56% of the world's population, and 79% of

individuals in developed countries live in cities by 2021 [1]. Since it is predicted that urban population growth will continue, with approximately 67% of the world's population will live in urban areas by 2050. Therefore, a better understanding of the complex processes at the intersection of urbanization, climate and human health is required [2].

*e-mail: mertakoglu@sdu.edu.tr

Urbanization is an anthropic change that creates changes in surface materials due to vegetation suppression, albedo variation and soil tightness, affecting the local energy balance, and contributing to the formation of the UHI [3]. Urbanization has been associated with an increase in the size and intensity of the UHI effect, which causes high levels of air pollution and heat, especially in summer [4, 5]. This effect is a result of the greater absorption of electromagnetic energy and the slow cooling of urbanized surfaces compared to surrounding areas with the presence of vegetation [3]. Many studies on Urban Cool Island (UCI), which aim to reduce the UHI effect with effective landscape planning, suggest that urban parks, which are an essential part of the urban forest, can achieve this by creating cool islands in a city [6-8]. Urban parks, considered an important part of the urban plant vegetation in cities, are an important urban green area that can form a "Park Cool Island (PCI)" cooler than the built-up areas around them [9-12]. The presence of urban parks can effectively improve the urban thermal environment and reduce the effects of UHI. Planning and design disciplines play a significant role in understanding how to design urban parks by paying attention to PCI density [12]. In the urbanization process, the change in Land Use/Land Cover (LULC), the natural landscape is replaced by urban texture, a pattern defined as urban warming and characterized by higher temperatures than the surrounding rural environment [13].

The urban heat island (UHI) effect is accepted as the most determinant heat accumulation phenomenon in the urban climate of the urban texture [14]. The urban temperature factor is one of the most critical factors affecting the urban climate, regulating and controlling various processes [15-17]. Studies on urban climate have shown that urban surfaces' thermal, optical and geometric properties absorb heat and affect the radiation properties, leading to the effect called UHI [13, 18]. Impervious surfaces that absorb more solar radiation are among the main factors in forming urban heat islands resulting from LULC transformation [19-21]. Urban Heat Islands can be characterized as surface urban heat islands (SUHI), referring to the land surface temperature and measuring the air temperature in the urban canopy layer [19, 22].

Previous research has discovered a relationship between the cooling effect of urban parks and vegetative properties [4, 10, 12, 23]. The surface characteristics of the designed urban park significantly affect the urban thermal environment [4, 24]. Many studies have found that green spaces' green lands or water bodies have a cooling effect [4, 8, 23]. PCI effect decreases linearly with the increase of urban park shape (perimeter/area) [25], and with increasing complexity in shape, the cooling effect of urban parks decreases [12].

Studies conducted over the past two decades have focused on the PCI density of urban park features. In these studies, it was seen that there was a positive correlation between PCI density and urban park size

[6, 8, 12, 25, 26]. In addition to studies focusing on the size of the urban park, studies have been conducted on the possibility of being related to other features of the park, such as urban forest structures [26]. Emphasizing the importance of urban park size as well as the shape of the urban park, the study states that urban park size is the most crucial factor affecting PCI density. Therefore, increasing urban park size could be an essential way to increase PCI density and reduce UHI impacts [12].

It has been observed that urban parks are, on average, 4.52°C (3.77°C) cooler than their surroundings during the summer (autumn) months, which confirms the term "urban cool islands" [12]. As a result of some studies, it is known that the PCI intensity measured by LST is higher than that measured by air temperature [10, 12, 26, 27]. Due to the PCI density that varies according to the seasons, it is seen that the cooler effect of the parks is higher than in other months, especially in summer. The fact that PCI density varies greatly between parks has shown that these differences may be related to urban park characteristics [12, 25, 28].

The studies show that plants' shading and transpiration properties in urban open green areas such as urban parks effectively reduce the air and surface temperature [29]. Plant material can alleviate the UHI effect by increasing the humidity in the air [30-32].

The UHI effect can be measured in two ways: by measuring the urban heat island effect in the air using the meteorological stations networks and by measuring the UHI at the surface temperature using remote sensing [33]. The current situation and time-dependent changes can be determined economically and quickly using Land Surface Temperature (LST) maps obtained using thermal remote sensing data. The data obtained with LST maps can be used in different applications, such as land cover and vegetation change analysis [34]. In his first study, Rao (1972) produced the land surface temperature map obtained with satellite thermal data and suggested that this data could measure the UHI effect [35].

Satellite remote sensing techniques use different wavelengths from the electromagnetic spectrum, such as visible near-infrared (VNIR) and shortwave infrared (SWIR) bands, to monitor the different types of land surfaces. Today, remote sensing spectral indexes, such as the NDVI, measure relative greenness [36] and the NDVI can be used as a general indicator of vegetation cover. NDVI is also helpful in determining the production of green vegetation and detecting vegetation changes [37].

In addition, thermal infrared (TIR) bands are also used to identify land surface temperature characteristics. The most popular index for vegetation in LST estimation is NDVI. High LST is associated with low vegetation in mixed urban terrain [38].

NDVI is used for different applications such as vegetation mapping, LULC, urban planning and LST monitoring [38-40]. LST deals with the UHI effect and changes significantly in an urban area [38, 41, 42]. It has

been found that there is a negative correlation between NDVI and LST [38, 43-46]. LST decreases with increasing vegetation [47]. In the twenty-first century, urban expansion and growth are responsible for creating urban heat islands or regions with high LST within the city [38, 48-50]. Following the decrease in green cover and construction increase, LST is doomed to increase. Green space is the basic need of any city as it is necessary for a healthy life and preserves the aesthetic and ecological beauty of urban areas [45].

When the climatic and topographic data of Ankara city center are evaluated, it is seen that the city center is gathered in an area remaining in a pit and forms a settlement network towards its surroundings. Ankara's this bowl-shaped model originating from the land structure, has taken the city away from the compact form over the years and transformed it into a form where dense construction is seen together. For all these reasons, a barrier has formed around the city and has revealed the heat island effect that prevents air flow. Studies show that Ankara is highly vulnerable to the effects of climate change. Especially in large cities such as Ankara, where urbanization is gradually increasing, it is observed that the heat island effect is felt more intensely day by day. In the "Climate Change Action Plan" published by Ankara Metropolitan Municipality, strategies and action plans have been developed to reduce the urban heat island effect. The importance of measuring and documenting the impact of smaller-scale urban parks on reducing the urban heat island has been emphasized in the strategies developed for the city [51-53].

This study aims to measure the effect of four city parks in Ankara on the urban heat island. In this study, LST calculations with Landsat 8 satellite data and NDVI calculations with Sentinel 2 satellite data were made using Google Earth Engine. The spatial resolution was changed to 10 m by resampling the LST map. In LST maps, zonal statistics such as standard deviation, minimum, maximum and mean values were calculated within five different zones.

Material and Methods

Study Area

Ankara is located between 39°38'81" and 40°02'30" North latitude and 32°31'20" and 33°05'06" East longitude in the Central Anatolia Region, dominated by plains formed by Kızılırmak and Sakarya Rivers. It is the capital of the Republic of Turkey. It is the third-largest city in Turkey, with an area of 25,437 km² and the second most populated city with a population of 5,747,325 people (Turkish Statistical Institute, 2022).

The average altitude above sea level of Ankara is 890 meters. In general, a continental climate is observed in Ankara. In addition to the steppe climate, Central Anatolia's climate, temperate and rainy climate characteristics are observed from the Black

Sea climate characteristics in the northern regions. In winter, there is much more rainfall than in summer. According to Köppen-Geiger, the climate is Csa (Hot Summer Mediterranean Climate). Monthly values of total precipitation, average, maximum, and minimum temperature were used for climatological analysis between 1975 and 2020 (Ankara Climate Change Action Plan, 2022).

The annual average temperature of Ankara is 11.9°C. The annual average rainfall is 393 mm. With 12 mm of precipitation, August is the driest month of the year. With an average of precipitation, the highest precipitation is seen in May. With a temperature of 23.4°C, August is the hottest month of the year. The average temperature in January is 0.2°C, the lowest average of the year. The amount of precipitation between the driest and wettest months of the year is 49 mm. The average temperature varies around 11°C throughout the year. The number of days with frost is 60-117, and the number of snowy days is 30.5 per year. The highest snow thickness was determined as 30 cm. The months with strong winds are March and April. The highest wind speed detected in Ankara is 29.2 m/s. According to the values measured for many years, the average pressure value of Ankara is 913.1 mbar, the highest-pressure value detected is 935.0 mbar, and the lowest pressure value is 891.0 mbar (Ankara Climate Change Action Plan, 2022).

The four oldest parks, which are of great importance to the city of Ankara, constitute the primary study areas of this study. The studied parks, including Altınpark, Gençlik Park, Kurtuluş Park and Botanik Park located in different parts of the Ankara urban area. To avoid the temperature differences depending on the synoptic weather conditions among the parks, the parks subjected for the present study were selected at the same elevations (840-890 m ASL) (Fig. 1). The characteristics of each park, such as the establishment years, parks total areas (m²), vegetation cover area (m²) and latitude-longitude are given in the (Table 1).

The workflow chart of the study is given in (Fig. 2). This study used Landsat 8 Level 2, Collection 2 Tier 1 and Sentinel 2 Level 2A data. NDVI and LST calculations were made using atmospherically corrected images in Google Earth Engine. For LST calculations, the open-source code published in Ermida et al. [54] was used using Landsat 8 Level 2, Collection 2 Tier 1 images. The LST algorithm we used in this study requires surface emissivity values for different surface characteristics. STER GEDv3 dataset of JPL is used for surface emissivity derivation for LST calculations [55]. Vegetation adjustment is applied using two different datasets of Landsat 8 NDVI and ASTER GEDv3 NDVI. Statistical Mono-Window (SMW) algorithm developed by the Climate Monitoring Satellite Application Facility (CM-SAF) is used for LST calculation. Because of the resolution advantage of Sentinel-2 images (10 m), NDVI maps were calculated with Sentinel-2. The spatial resolution, which was 30 meters, was up-sampled (using nearest neighbour interpolation technique) to 10 meters

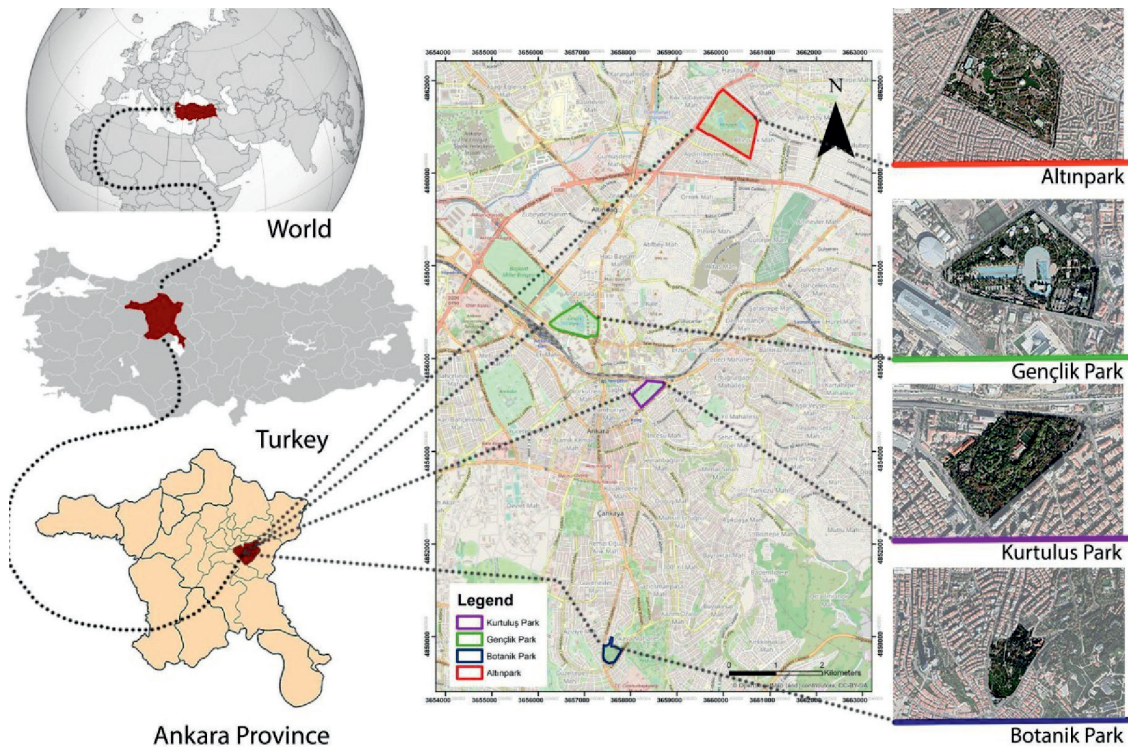


Fig. 1. Location map.

Table 1. The characteristics of parks.

Park Names	Established (year)	Park Total Area (m ²)	Vegetation Cover (m ²)	Vegetation Cover/Total area (%)	Latitude/ Longitude
Altınpark	1987	606,591	353,063	58	39°58'0"N/32°52'59"E
Gençlik Park	1936	278,487	146,951	53	39°56'13"N/32°51'2"E
Kurtuluş Park	1957	120,506	100,629	84	39°55'36"N/32°51'50"E
Botanik Park	1970	65,000	46,223	71	39°58'03"N/32°52'31"E

to use with the LST maps. Buffer zones were determined using the literature on LST maps, and zonal statistics (min, max, mean, stdev) were calculated to evaluate these zones (Table 2).

Data

Sentinel 2 Level 2A and Landsat 8 Level 2, Collection 2 Tier 1 image were used in this study. Sentinel 2 Level 2A image has a date of 20.07.2021, and Landsat 8 Level 2, Collection 2 Tier 1 image has a date of 15.07.2021. Since Landsat 8 and Sentinel 2 don't have the same satellite period and orbit, satellite images taken at the two closest dates were used. Since there is no vegetation period change, this 5-day difference does not affect the analysis.

NDVI

NDVI is a standardized index that allows you to create an image of vegetation (relative biomass).

This index takes advantage of the contrast of the features of the two bands from a multiband raster dataset. These are the absorptions of chlorophyll pigment in the red band and the high reflectivity of plant materials in the near-infrared (NIR) band. The NDVI range is -1 to $+1$. A higher value of NDVI means healthy and dense vegetation. Low NDVI values indicate sparse vegetation. The NDVI is calculated from Eq. (1):

$$NDVI = \frac{NIR - RED}{NIR + RED} \quad (1)$$

RED and NIR represent spectral reflection measurements obtained in red (visible) and near-infrared regions [56].

The NDVI is used to calculate the fraction of vegetation cover (FVC), and in this study, we derive this by using Carlson and Ripley [57] formula is in Eq. (2):

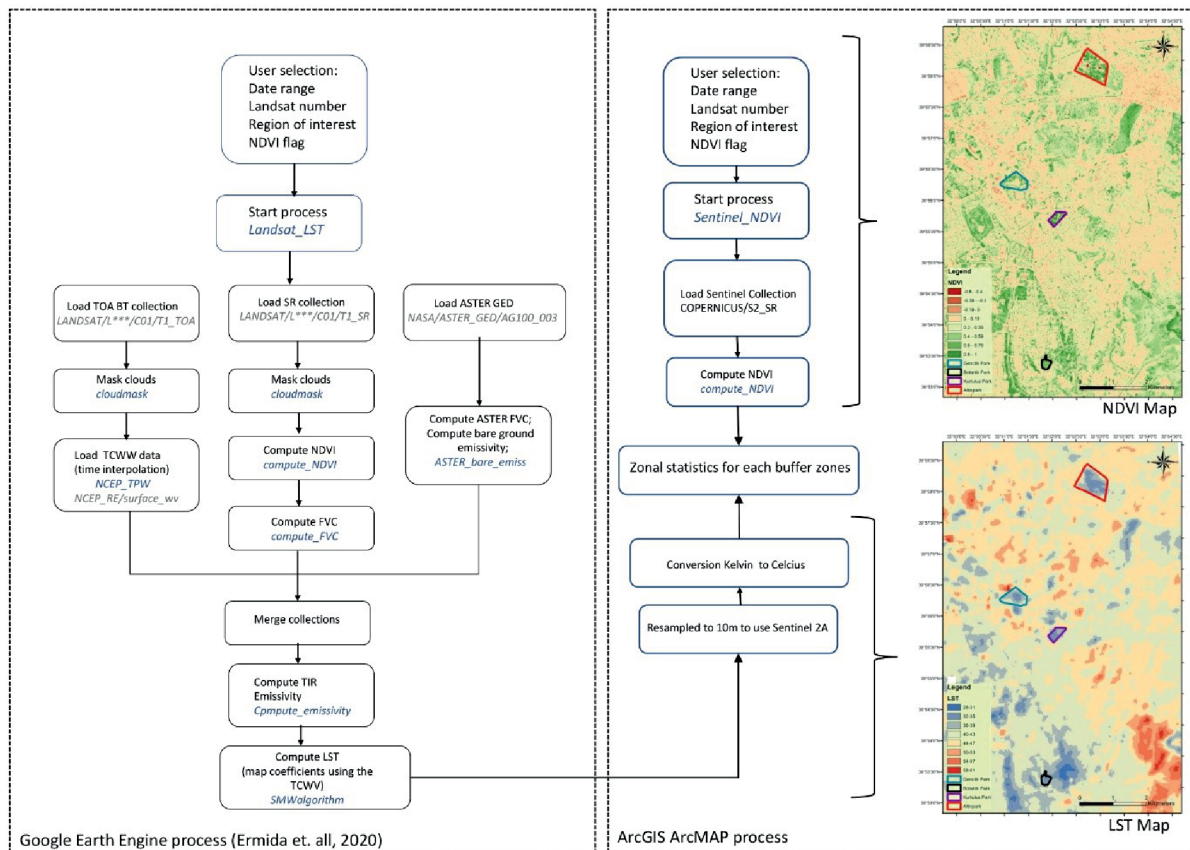


Fig. 2. Work-flow chart.

$$FVC = \left(\frac{NDVI - NDVI_{bare}}{NDVI_{veg} - NDVI_{bare}} \right)^2 \quad (2)$$

In this formula, $NDVI_{bare}$ and $NDVI_{veg}$ indicate completely bare and vegetated pixels. Based on the literature [58], these threshold values are based on $NDVI_{bare} = 0.2$ and $NDVI_{veg} = 0.86$, respectively.

LST

LST is defined as the surface temperature of the ground. The LST measures radiation emission from the land surface, where incoming solar energy warms the earth, or from the canopy surface in areas with vegetation.

In this study, LST maps were calculated using Google Earth Engine, with the method and process prepared by [54]. This method uses SMW algorithms to derive LST based on the empirical relationship between TOA brightness temperature in a single TIR channel and LST by utilizing linear regression [59-61]. The LST is calculated from Eq. (3),

$$LST = A_i \frac{T_b}{\epsilon} + B_i \frac{1}{\epsilon} + C_i \quad (3)$$

In this formula, T_b is the TOA brightness temperature in the TIR channel, and ϵ is the surface

emissivity. Algorithm coefficients A_i , B_i ; and C_i are determined from linear regressions of radiative transfer simulations performed for 10 TCWV classes ($I = 1, \dots, 10$) ranging from 0 to 6 cm in 0.6 cm steps, and TCWV values above 6 cm are assigned to last class.

Relationship between LST and NDVI

Studies show a strong correlation between NDVI and LST [62, 63]. Especially in summer, NDVI values increase in vegetated areas [64]. The decrease in NDVI values causes an increase in LST values [65]. It can be observed that there is a one-to-one and negative correlation between the vegetated areas and the LST [66, 67].

Zonal Statistics

Regions which can be defined by a vector dataset based on values from another (raster) dataset are used to calculate zonal statistics. The input zone dataset calculates a single output value for each zone. The zonal statistics tool calculates list of the statistics for a given input, a subset, or a single statistic but outputs the result as a table rather than a raster output. Statistics calculated in ArcGIS (Arcmap 10. 6. 1) from NDVI and LST data for this study consist of standard deviation, maximum, minimum, and mean values. In addition to the values

inside the park, statistical data of 4 separate 50-meter buffer zones were calculated and compared.

Results and Discussion

The increasing rate of urbanization which is thought to have become a necessity with the increase in population in cities, threatens green areas with each passing day and causes changes in the microclimate scale of the cities. Urban heat islands are formed due to the materials used on hard surfaces, which replace green areas, absorbing heat and trapping it in cities. The urban heat island effect, first described in the 1800s, reveals

that urban areas are warming more than rural areas. Due to the intense population growth, Ankara is at the forefront of our cities' rapid urbanization. It is seen that there are changes in the urban climate parameters of Ankara as a result of intense construction. To solve the problem, it is essential to determine the size of the urban heat island effect at the beginning of the studies. With the urban heat island effect reaching global dimensions, developing strategies ranging from lower to upper scale and transforming them into action plans to solve the problem is necessary. It should be known that the cities' socio-economic structure, cultural conditions, and physical conditions, such as their morphology and land use, are also effective in determining and

Table 2. LST-NDVI summary graph of parks.

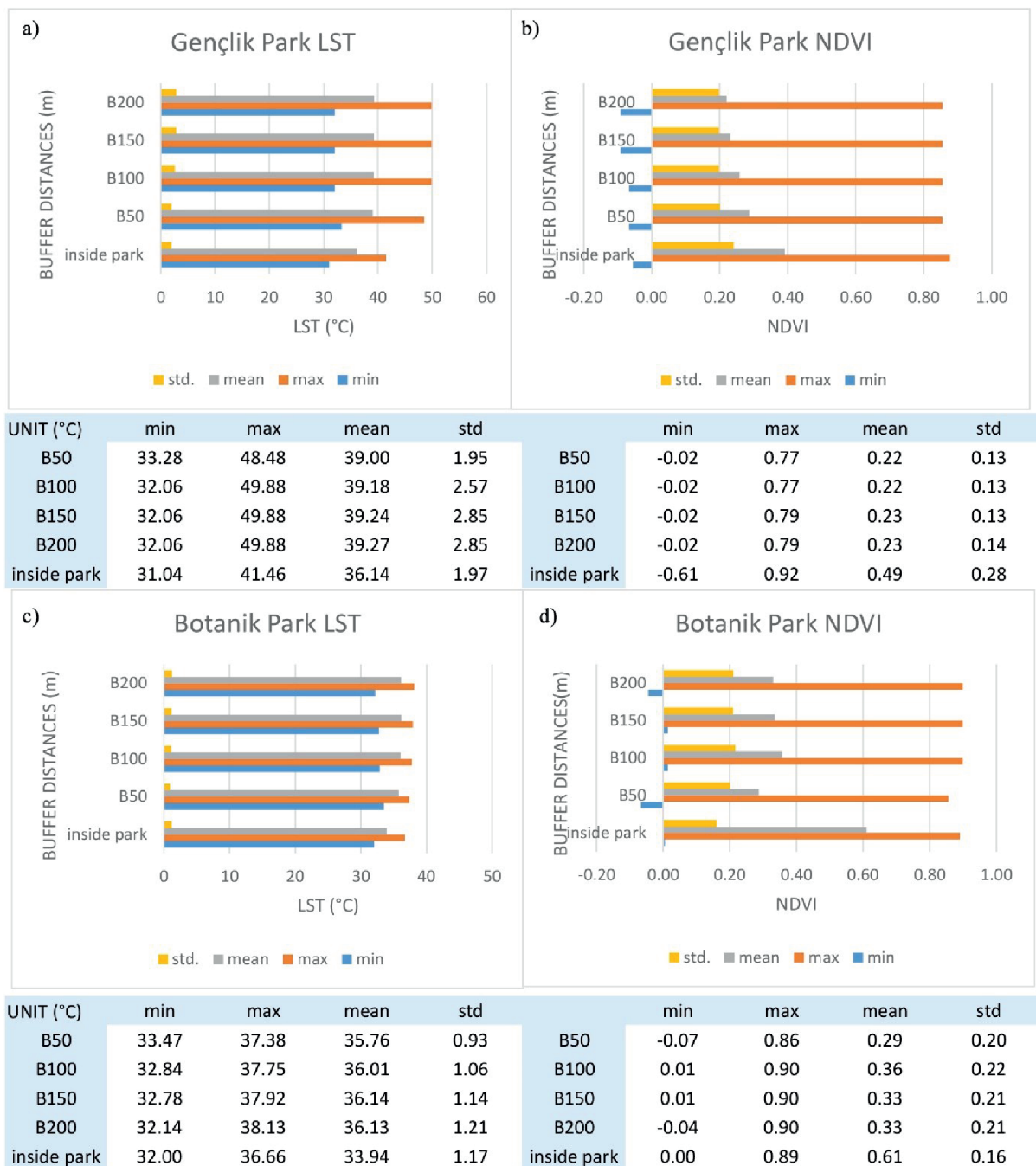


Table 2. Continued.



measuring the urban heat island. With the developing technology and information infrastructure, studies in this field are increasing with significant momentum. The availability of remote sensing and satellite technologies provides a significant advantage in terms of time, while considerable savings are achieved in the budget.

In his study, Bilgili [68] stated that “The effects of micro-scale climate change caused by green areas within their borders and in their immediate surroundings vary according to the spatial (size), structural (pattern and plant species) and temporal (phenological periods) characteristics of the green areas. Therefore, the contribution of green areas to the urban ecosystem is

a dynamic situation that emerges with the combined effects of these areas’ spatial, structural and temporal characteristics.

NDVI, LST and Zonal Statistics calculations were made for all parks using the methods mentioned in the materials and methods. Since these parks have different land use characteristics, NDVI and LST values for each park show differences (Fig. 3).

NDVI

NDVI values calculated for each park are grouped and given in the (Fig. 3). NDVI values in plant parts

of Altınpark vary between 0.4 and 1. There are healthy plants in the area and the hard surfaces. NDVI values range from -0.6 to 0.2 in parts with hard surfaces. Since

Altınpark is located in a densely populated area, there is a significant change in NDVI values starting from the park boundaries (Table 2f).

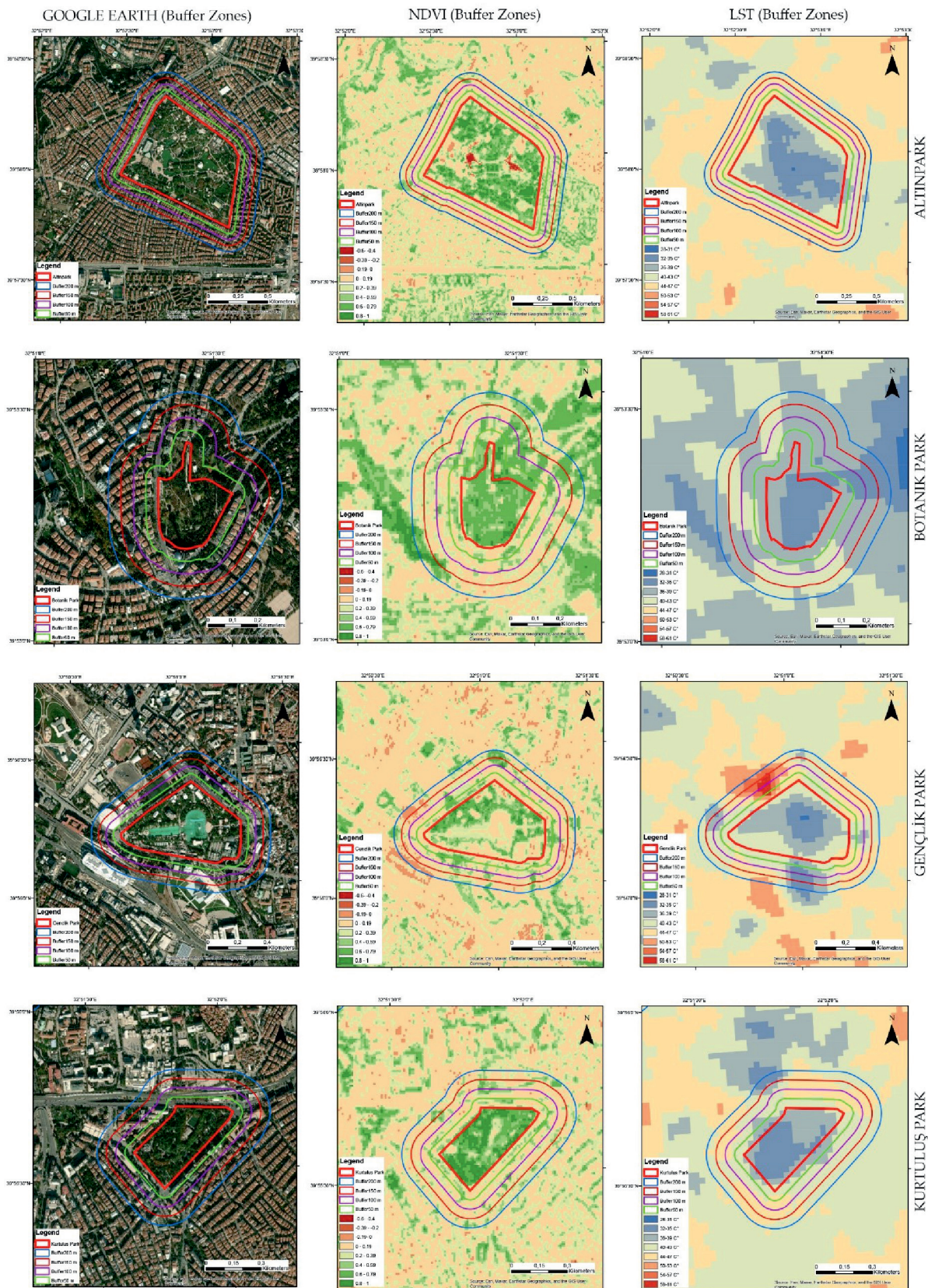


Fig. 3. GOOGLE EARTH-LST-NDVI Maps of Urban Parks (buffer zones).

Botanik Park has been seen as one of the parks with more green areas within the park boundaries, such as Kurtuluş Park. NDVI values in this park ranged from 0.2 to 1 (Table 2d).

NDVI values in Gençlik Park vary between 0.4 and 1. It has been determined that the amount of green space in Gençlik Park is less than Altınpark. In this park, where the hard ground is high, NDVI values varied between -0.2 and 0.2 (Table 2b).

Kurtuluş Park has more green areas than Altınpark and Gençlik Park, considering the total area. NDVI values in this park range from 0 to 1 (Table 2h).

While vegetation was healthier in Gençlik Park and Botanik Park, when the number of plants was evaluated according to the park borders, both the number of plants and the number of healthy plants were found to be less in Altınpark and Gençlik Park .

LST

LST values calculated for each park are grouped and given in the Fig. 3. When the surface temperatures of each park are evaluated.

Regions with dense vegetation are at lower temperatures in Altınpark. The temperature increases as you go from the park's centre to the park's boundaries.

Since there is a pool in Gençlik Park, even if the amount of green space is low, it is seen that the part where the pool is located and its surroundings have a lower temperature than the other parts.

Due to the amount of green space in Kurtuluş Park has a lower temperature within the park's boundaries.

Botanik Park by having much healthier vegetation cover like Gençlik Park, generally has low temperatures. Another reason for this is that it is located in the valley.

Zonal Statistics

After NDVI and LST calculations for each park, Zonal Statistics calculations were performed and summarized in Table 2.

Different buffer distances were used according to the area's characteristics in various studies in the literature [69]. After examining the LST maps, this study decided to create four buffer zones of 50 meters. [68] In this study, findings show that 1°C difference as they move away from the parks by 50 and 200 m (Fig.3). This situation was considered when creating buffer zones.

The LST buffer zones created around Altınpark show that this park has a higher temperature increase effect than other parks. As the buffer distance increases, the temperature rises. The temperature rises 3.5°C for the buffer created 50 meters from the park boundary. The change in buffer zones outside the park is around 1°C (Table 2e).

There is a 3°C difference between the LST values of the Gençlik Park in the park and the LST values of the buffer zones created around the park (Table 2a). As you

move away from the park, the temperature rises in some areas. In areas 50 meters away from the park boundary, there is a 3°C increase in temperature. The temperature difference between the buffer zones outside the park is around 0.3°C.

When the LST values in and around Kurtuluş Park were examined, it was seen that the temperature values of the first 50-meter buffer zone were higher than the temperature inside the park. Although it is seen that the temperature change is affected in areas after 100 m in some regions, it has not been taken into account since they are very small regions. At a distance of 50 meters from the park boundary, the temperature increase is about 3°C (Table 2g).

When Botanik Park and its surroundings are examined, it is seen that the temperature in the park continues to increase around the park. The temperature rises about 2°C in 50 meters surroundings of the park. Unlike other parks, the temperature around the park increased to lower degrees. It is considered that this is because the park is in the valley (Table 2c).

Conclusion

This study investigated the effect of four city parks in Ankara on the urban heat island using remote sensing and GIS techniques, LST and NDVI values calculated using Google Earth Engine by analyzing Landsat 8 and Sentinel-2 images. LST values of selected buffer zones in and around the park were determined by zonal analysis of LST values on Arcmap.

It is seen in the analysis and NDVI maps that the parks have dense green areas. LST values, negatively correlated with NDVI, were lower in the park but higher in buffer zones away from the park. The 50-meter buffer zone, the first buffer zone after the park borders, is the buffer zone where the temperature change is the highest at approximately 3°C compared to the inside of the park. The temperature variation between the other buffer zones was not considerable. As a result, the urban heat island effect caused an increase in the temperature of the city of Ankara.

Considering the temperature changes around the urban parks in the city, it is seen that these parks reduce the city's temperature locally.

The results obtained in this study are important for decision makers to investigate some indicators that can be used in urban planning and in selecting the location of parks.

Conflict of Interest

The authors declare no conflicts of interest.

References

1. World Population Data Sheet 2021. Retrieved from <https://interactives.prb.org/2021-wpds/wp-content/uploads/2021/08/letter-booklet-2021-world-population.pdf> **2021**.
2. DEBBAGE N., SHEPHERD J.M. The urban heat island effect and city contiguity. *Computers, Environment and Urban Systems*, 54, 181, **2015**.
3. DE ALMEIDA C.R., TEODORO A.C., GONÇALVES A. Study of the urban heat island (Uhi) using remote sensing data/techniques: A systematic review. *Environments - MDPI*, 8 (10), 1, **2021**.
4. WANG X., CHENG H., XI J., YANG G., ZHAO Y. Relationship between Park Composition, Vegetation Characteristics and Cool Island Effect. *Sustainability*, 10 (3), 587, **2018**.
5. SANTAMOURIS M., HADDAD S., FIORITO F., OSMOND P., DING L., PRASAD D., WANG R. Urban heat island and overheating characteristics in Sydney, Australia. An analysis of multiyear measurements. *Sustainability (Switzerland)*, 9 (5), **2017**.
6. LIN W., YU T., CHANG X., WU W., ZHANG Y. Calculating cooling extents of green parks using remote sensing: Method and test. *Landscape and Urban Planning*, 134, 66, **2015**.
7. DU H., CAI W., XU Y., WANG Z., WANG Y., CAI Y. Quantifying the cool island effects of urban green spaces using remote sensing Data. *Urban Forestry and Urban Greening*, 27, 24, **2017**.
8. CAO X., ONISHI A., CHEN J., IMURA H. Quantifying the cool island intensity of urban parks using ASTER and IKONOS data. *Landscape and Urban Planning*, 96 (4), 224, **2010**.
9. CHEN Y., WONG N.H. Thermal benefits of city parks. *Energy and Buildings*, 38 (2), 105, **2006**.
10. JAUREGUI E. Influence of a large urban park on temperature and convective precipitation in a tropical city. *Energy and Buildings*, 15 (3-4), 457, **1990**.
11. KARDINAL JUSUF S., WONG N.H., HAGEN E., ANGGORO R., HONG Y. The influence of land use on the urban heat island in Singapore. *Habitat International*, 31 (2), 232, **2007**.
12. REN Z., HE X., ZHENG H., ZHANG D., YU X., SHEN G., GUO R. Estimation of the relationship between urban park characteristics and park cool island intensity by remote sensing data and field measurement. *Forests*, 4 (4), 868, **2013**.
13. FEYISA G.L., DONS K., MEILBY H. Efficiency of parks in mitigating urban heat island effect: An example from Addis Ababa. *Landscape and Urban Planning*, 123, 87, **2014**.
14. OKE T.R. *Atmospheric Environment* Pergamon Press **7, 1973**.
15. BLOCKEN B., STATHOPOULOS T., CARMELIET J. CFD simulation of the atmospheric boundary layer: wall function problems. *Atmospheric Environment*, 41 (2), 238, **2007**.
16. PICKETT S.T.A., CADENASSO M.L., GROVE J.M., NILON C.H., POUYAT R.V., ZIPPERER W.C., COSTANZA R. Urban ecological systems: Linking terrestrial ecological, physical, and socioeconomic components of metropolitan areas. *Annual Review of Ecology and Systematics*, 32, 127, **2001**.
17. YANG L., QIAN F., SONG D.X., ZHENG K.J. Research on Urban Heat-Island Effect. In *Procedia Engineering* **169, 11, Elsevier Ltd. 2016**.
18. VOOGT J.A., OKE T.R. Thermal remote sensing of urban climates. *Remote Sensing of Environment*, 86 (3), 370, **2003**.
19. LI Z., XIE C., CHEN D., LU H., CHE S. Effects of Land Cover Patterns on Land Surface Temperatures Associated with Land Use Types along Urbanization Gradients in Shanghai, China. *Polish Journal of Environmental Studies*, 29 (1), 713, **2020**.
20. MUSHORE T.D., MUTANGA O., ODINDI J., DUBE T. Determining extreme heat vulnerability of Harare Metropolitan City using multispectral remote sensing and socio-economic data. <https://doi.org/10.1080/14498596.2017.1290558>, 63 (1), 173, **2017**.
21. SONG Y., WU C. Examining the impact of urban biophysical composition and neighboring environment on surface urban heat island effect. *Advances in Space Research*, 57 (1), 96, **2016**.
22. XIE M., WANG Y., CHANG Q., FU M., YE M. Assessment of landscape patterns affecting land surface temperature in different biophysical gradients in Shenzhen, China. *Urban Ecosystems*, 16 (4), 871, **2013**.
23. SUN R., CHEN L. How can urban water bodies be designed for climate adaptation? *Landscape and Urban Planning*, 105 (1-2), 27, **2012**.
24. GAGE E.A., COOPER D.J. Urban forest structure and land cover composition effects on land surface temperature in a semi-arid suburban area. *Urban Forestry and Urban Greening*, 28, 28, **2017**.
25. BLACHOWSKI J., HAJNRYCH M. Assessing the cooling effect of four urban parks of different sizes in a temperate continental climate zone: Wrocław (poland). *Forests*, 12 (8), **2021**.
26. CHANG C.R., LI M.H., CHANG S.D. A preliminary study on the local cool-island intensity of Taipei city parks. *Landscape and Urban Planning*, 80 (4), 386, **2007**.
27. BOWLER D.E., BUYUNG-ALI L., KNIGHT T.M., PULLIN A.S. Urban greening to cool towns and cities: A systematic review of the empirical evidence. *Landscape and Urban Planning*. Elsevier. **2010**.
28. OLIVEIRA S., ANDRADE H., VAZ T. The cooling effect of green spaces as a contribution to the mitigation of urban heat: A case study in Lisbon. *Building and Environment*, 46 (11), 2186, **2011**.
29. HOWE D.A., HATHAWAY J.M., ELLIS K.N., MASON L.R. Spatial and temporal variability of air temperature across urban neighborhoods with varying amounts of tree canopy. *Urban Forestry and Urban Greening*, 27 (April), 109, **2017**.
30. TAHA H. Urban climates and heat islands: Albedo, evapotranspiration, and anthropogenic heat. *Energy and Buildings*, 25 (2), 99, **1997**.
31. XIAO X.D., DONG L., YAN H., YANG N., XIONG Y. The influence of the spatial characteristics of urban green space on the urban heat island effect in Suzhou Industrial Park. *Sustainable Cities and Society*, 40, 428, **2018**.
32. JIANG J., TIAN G. Analysis of the impact of Land use/Land cover change on Land Surface Temperature with Remote Sensing. *Procedia Environmental Sciences*, 2 (5), 571, **2010**.
33. STREUTKER D.R. Satellite-measured growth of the urban heat island of Houston, Texas. *Remote Sensing of Environment*, 85 (3), 282, **2003**.

34. MERCAN Ç. Türkiye Uzaktan Algılama Dergisi Yer Yüze Sıcaklığının Termal Uzaktan Algılama Görüntüleri ile Araştırılması: Muş İli Örneği Investigation of Land Surface Temperature with Thermal Remote Sensing Images: A Case Study Muş Province, 2 (2), 42, 2020.
35. KHORRAMI B., GUNDUZ O. Uzaktan Algılama ve CBS' nin Yüze Sıcaklığı ve Kentsel Isı Adası Tespit ve Analizinde Uygulanması. In Meteorolojik Uzaktan Algılama Sempozyumu (UZALMET 2019) Antalya, Türkiye. 2019.
36. RAYNOLDS M.K., COMISO J.C., WALKER D.A., VERBYLA D. Relationship between satellite-derived land surface temperatures, arctic vegetation types, and NDVI. Remote Sensing of Environment, 112 (4), 1884, 2008.
37. GANDHI G.M., PARTHIBAN S., THUMMALU N., CHRISTY A. Ndvi: Vegetation Change Detection Using Remote Sensing and Gis - A Case Study of Vellore District. In Procedia Computer Science 57, 1199, Elsevier. 2015.
38. GUHA S. Dynamic seasonal analysis on LST-NDVI relationship and ecological health of Raipur City, India. Ecosystem Health and Sustainability, 7 (1), 2021.
39. DU S., XIONG Z., WANG Y.C., GUO L. Quantifying the multilevel effects of landscape composition and configuration on land surface temperature. Remote Sensing of Environment, 178, 84, 2016.
40. MONDAL A., GUHA S., MISHRA PRABHASH K., KUNDA S. Land use/Land cover changes in Hugli Estuary using Fuzzy C-Mean algorithm. International Journal of Geomatics and Geosciences., 2 (2), 613, 2011.
41. HAO X., LI W., DENG H. The oasis effect and summer temperature rise in arid regions - Case study in Tarim Basin. Scientific Reports, 6 (June), 1, 2016.
42. TRAN D.X., PLA F., LATORRE-CARMONA P., MYINT S.W., CAETANO M., KIEU H.V. Characterizing the relationship between land use land cover change and land surface temperature. ISPRS Journal of Photogrammetry and Remote Sensing, 124, 119, 2017.
43. ABDULMANA S., LIM A., WONGSAI S., WONGSAI N. Land surface temperature and vegetation cover changes and their relationships in Taiwan from 2000 to 2020. Remote Sensing Applications: Society and Environment, 24, 100636, 2021.
44. GUHA S., GOVIL H., TALOOR A.K., GILL N., DEY A. Land surface temperature and spectral indices: A seasonal study of Raipur City. Geodesy and Geodynamics, 13 (1), 72, 2022.
45. KUMARI B., TAYYAB M., SHAHFAHAD, SALMAN, MALLICK J., KHAN M.F., RAHMAN, A. Satellite-Driven Land Surface Temperature (LST) Using Landsat 5, 7 (TM/ETM+ SLC) and Landsat 8 (OLI/TIRS) Data and Its Association with Built-Up and Green Cover Over Urban Delhi, India. Remote Sensing in Earth Systems Sciences, 1 (3-4), 63, 2018.
46. YUE W., XU J., TAN W., XU L. The relationship between land surface temperature and NDVI with remote sensing: Application to Shanghai Landsat 7 ETM+ data. International Journal of Remote Sensing, 28 (15), 3205, 2007.
47. TETALI S., BAIRD N., KLIMA K. A multicity analysis of daytime Surface Urban Heat Islands in India and the US. Sustainable Cities and Society, 77, 103568, 2022.
48. FU P., WENG Q. A time series analysis of urbanization induced land use and land cover change and its impact on land surface temperature with Landsat imagery. Remote Sensing of Environment, 175, 205, 2016.
49. LIU Y., PENG J., WANG Y. Efficiency of landscape metrics characterizing urban land surface temperature. Landscape and Urban Planning, 180, 36, 2018.
50. PENG J., JIA J., LIU Y., LI H., WU J. Seasonal contrast of the dominant factors for spatial distribution of land surface temperature in urban areas. Remote Sensing of Environment, 215, 255, 2018.
51. ÇIÇEK İ., DOĞAN U. Detection of Urban Heat Island in Ankara, Turkey. Coğrafi Bilimler Dergisi, 3 (1), 57, 2005.
52. DIHKAN M., KARSLI F., GUNEROGLU N., GUNEROGLU A. Evaluation of urban heat island effect in Turkey. Arabian Journal of Geosciences, 11 (8), 2018.
53. YÜKSEL Ü., YILMAZ O. Ankara Kentinde Kentsel Isı Adası Etkisinin Yaz Aylarında Uzaktan Algılama ve Meteorolojik Gözlemlere Dayalı Olarak Saptanması Ve Değerlendirilmesi Üzerinde Bir Araştırma. Gazi Üniversitesi Mühendislik Mimarlık Fakültesi Dergisi, 23 (4), 937. Retrieved from <https://dergipark.org.tr/pub/gazimmfd/issue/6678/88558> 2008.
54. ERMIDA S.L., SOARES P., MANTAS V., GÖTTSCHE F.M., TRIGO I.F. Google earth engine open-source code for land surface temperature estimation from the landsat series. Remote Sensing, 12 (9), 1471, 2020.
55. HULLEY G.C., HOOK S.J., ABBOTT E., MALAKAR N., ISLAM T., ABRAMS M. The ASTER Global Emissivity Dataset (ASTER GED): Mapping Earth's emissivity at 100 meter spatial scale. Geophysical Research Letters, 42 (19), 7966, 2015.
56. HURCOM S.J., HARRISON A.R. The NDVI and spectral decomposition for semi-arid vegetation abundance estimation. International Journal of Remote Sensing, 19 (16), 3109, 1998.
57. CARLSON T.N., RIPLEY D.A. On the relation between NDVI, fractional vegetation cover, and leaf area index. Remote Sensing of Environment, 62 (3), 241, 1997.
58. JIMÉNEZ-MUÑOZ J.C., SOBRINO J.A., PLAZA A., GUANTER L., MORENO J., MARTÍNEZ P. Comparison between fractional vegetation cover retrievals from vegetation indices and spectral mixture analysis: Case study of PROBA/CHRIS data over an agricultural area. Sensors, 9 (2), 768, 2009.
59. SUN D., PINKER R.T., BASARA J.B. Land surface temperature estimation from the next generation of Geostationary Operational Environmental Satellites: GOES M-Q. Journal of Applied Meteorology, 43 (2), 363, 2004.
60. FREITAS S.C., TRIGO I.F., MACEDO J., BARROSO C., SILVA R., PERDIGÃO R. Land surface temperature from multiple geostationary satellites. International Journal of Remote Sensing, 34 (9-10), 3051, 2013.
61. LI Z.L., TANG B.H., WU H., REN H., YAN G., WAN Z., SOBRINO J.A. Satellite-derived land surface temperature: Current status and perspectives. Remote Sensing of Environment, 131, 14, 2013.
62. KAUFMANN R.K., ZHOU L., MYNENI R.B., TUCKER C.J., SLAYBACK D., SHABANOV N.V., PINZON J. The effect of vegetation on surface temperature: A statistical analysis of NDVI and climate data. Geophysical Research Letters, 30 (22), 2147, 2003.
63. CHEN X.L., ZHAO H.M., LI P.X., YIN Z.Y. Remote sensing image-based analysis of the relationship between urban heat island and land use/cover changes. Remote Sensing of Environment, 104 (2), 133, 2006.
64. JULIEN Y., SOBRINO J.A., VERHOEF W. Changes in land surface temperatures and NDVI values over Europe

- between 1982 and 1999. *Remote Sensing of Environment*, 103 (1), 43, **2006**.
65. BOKAIE M., ZARKESH M.K., ARASTEH P.D., HOSSEINI A. Assessment of Urban Heat Island based on the relationship between land surface temperature and Land Use/Land Cover in Tehran. *Sustainable Cities and Society*, 23 (23), 94, **2016**.
66. LI W., BAI Y., CHEN Q., HE K., JI X., HAN C. Discrepant impacts of land use and land cover on urban heat islands: A case study of Shanghai, China. *Ecological Indicators*, 47, 171, **2014**.
67. KAPLAN G., AVDAN U., AVDAN Z.Y. Urban Heat Island Analysis Using the Landsat 8 Satellite Data: A Case Study in Skopje, Macedonia. *Proceedings 2018*, Vol. 2, Page 358, 2 (7), 358, **2018**.
68. BILGILI B.C., ŞAHİN Ş., YILMAZ O., GÜRBÜZ F., ARICI Y.K. Temperature distribution and the cooling effects on three urban parks in Ankara, Turkey. *International Journal of Global Warming*, 5 (3), 296, **2013**.
69. ZHAO Z.Q., HE B.J., LI L.G., WANG H.B., DARKO A. Profile and concentric zonal analysis of relationships between land use/land cover and land surface temperature: Case study of Shenyang, China. *Energy and Buildings*, 155, 282, **2017**.